Evolution of Enzymatic Activities in the Enolase Superfamily: D-Tartrate Dehydratase from *Bradyrhizobium japonicum*[†,‡]

Wen Shan Yew,[§] Alexander A. Fedorov,[||] Elena V. Fedorov,[||] Bryant McKay Wood,[§] Steven C. Almo,*[,||] and John A. Gerlt*[,§]

Departments of Biochemistry and Chemistry, University of Illinois at Urbana−Champaign, 600 South Mathews Avenue, Urbana, Illinois 61801, and Department of Biochemistry, Albert Einstein College of Medicine, Bronx, New York 10461

Received August 18, 2006; Revised Manuscript Received September 18, 2006

ABSTRACT: We focus on the assignment of function to and elucidation of structure−function relationships for a member of the mechanistically diverse enolase superfamily encoded by the *Bradyrhizobium japonicum* genome (bll6730; GI:27381841). As suggested by sequence alignments, the active site contains the same functional groups found in the active site of mandelate racemase (MR) that catalyzes a 1,1-proton transfer reaction: two acid/base catalysts, Lys 184 at the end of the second β-strand, and a His 322-Asp 292 dyad at the ends of the seventh and sixth β-strands, respectively, as well as ligands for an essential Mg^{2+}, Asp 213, Glu 239, and Glu 265 at the ends of the third, fourth, and fifth β-strands, respectively. We screened a library of 46 acid sugars and discovered that only D-tartrate is dehydrated, yielding oxaloacetate as product. The kinetic constants ($k_{cat} = 7.3\ s^{-1}$; $k_{cat}/K_M = 8.5 \times 10^4\ M^{-1}\ s^{-1}$) are consistent with assignment of the D-tartrate dehydratase (TarD) function. The kinetic phenotypes of mutants as well as the structures of liganded complexes are consistent with a mechanism in which Lys 184 initiates the reaction by abstraction of the α-proton to generate a Mg^{2+}-stabilized enediolate intermediate, and the vinylogous β-elimination of the 3-OH group is general acid-catalyzed by the His 322, accomplishing the anti-elimination of water. The replacement of the leaving group by solvent-derived hydrogen is stereorandom, suggesting that the enol tautomer of oxaloacetate is the product; this expectation was confirmed by its observation by ^1H NMR spectroscopy. Thus, the TarD-catalyzed reaction is a "simple" extension of the two-step reaction catalyzed by MR: base-catalyzed proton abstraction to generate a Mg^{2+}-stabilized enediolate intermediate followed by acid-catalyzed decomposition of that intermediate to yield the product.

The members of the enolase superfamily of mechanistically diverse enzymes catalyze reactions that are initiated by general base-catalyzed abstraction of a proton from a carbon adjacent to a carboxylate group to generate an enediolate intermediate; this intermediate is rendered kinetically competent by coordination to an essential Mg^{2+} (*1*−*3*). The intermediate is directed to the product with the participation of a general acid catalyst. The homologous members of the superfamily share a bidomain structure: residues involved in determining substrate specificity are located in a capping domain formed from N- and C-terminal segments of the polypeptide; the acid/base catalysts and ligands for the metal ion are located at the ends of the β-strands in a $(\beta/\alpha)_7\beta$-barrel [modified $(\beta/\alpha)_8$-barrel] domain.

The members of the enolase superfamily are partitioned into subgroups based on the identities of the acid/base catalysts and the metal ion ligands. The members of the muconate lactonizing enzyme (MLE)[1] subgroup *always* share conserved, structurally opposed Lys residues at the ends of the second and sixth β-strands. The known reactions catalyzed by members of the MLE subgroup are MLE (*4*), *o*-succinylbenzoate synthase (*4*), L-Ala-D/L-Glu epimerase (*5*), and *N*-succinylamino acid racemase (*6*).

The members of the mandelate racemase (MR) subgroup *always* share a conserved, hydrogen-bonded dyad between a His positioned at the end of the seventh β-strand and an Asp positioned at the end of the sixth β-strand. Often, an acid/base functional group is also located at the end of the second β-strand so that acid/base chemistry can occur on both faces of the bound substrate and Mg^{2+}-stabilized enediolate intermediate. However, our recent sequence analyses suggest that a variety of acid/base functional groups can be located at the end of the second β-strand, including Arg, His, or Tyr, as well as the Lys that is present in the prototypic MR. The known reactions catalyzed by members of the MR subgroup are MR (*4*), D-glucarate dehydratase (GlucD) (*4*), D-galactonate dehydratase (GalD) (*7*, *8*), and L-fuconate dehydratase (FucD) (*9*).

[†] This research was supported by Grant GM-52594 and Program Project Grant GM-71790 from the National Institutes of Health.

[‡] The X-ray coordinates and structure factors for wild-type TarD liganded only with Mg^{2+}, wild-type TarD liganded with Mg^{2+} and *meso*-tartrate, and the K184A mutant liganded with Mg^{2+} and D-tartrate have been deposited in the Protein Data Bank (PDB accession codes 1TZZ, 2DW7, and 2DW6, respectively).

* Corresponding authors. J.A.G.: phone, (217) 244-7414; fax, (217) 244-6538; e-mail, j-gerlt@uiuc.edu. S.C.A.: phone, (718) 430-2746; fax, (718) 430-8565; e-mail: almo@aecom.yu.edu.

[§] University of Illinois at Urbana−Champaign.

[||] Albert Einstein College of Medicine.

[1] Abbreviations: FucD, L-fuconate dehydratase; GalD, D-galactonate dehydratase; GlucD, D-glucarate dehydratase; MDH, L-malate dehydrogenase; MLE, muconate lactonizing enzyme; MR, mandelate racemase; TarD, D-tartrate dehydratase.

10.1021/bi061688g CCC: $33.50
Published on Web 11/14/2006

Scheme 1

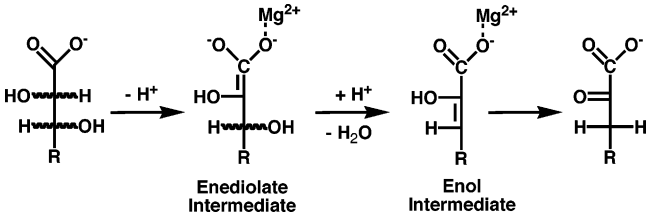

MR, the prototype for the MR subgroup, has two acid/base catalysts: Lys 166 at the end of the second β-strand and the conserved His 297-Asp 270 dyad. Extensive functional and structural investigations have allowed a detailed understanding of the mechanism of the MR-catalyzed 1,1-proton transfer reaction (*10*). The structurally opposed acid/base catalysts mediate proton transfers to and from the α-carbon of the substrate via the Mg^{2+}-coordinated enediolate intermediate to accomplish racemization.

The sequence databases now contain >600 members of the MR subgroup; based on sequence alignments, more than 230 are predicted to share the same acid/base functional groups and metal ion ligands found in MR (J. A. Gerlt, unpublished observations). On the basis of sequence homology and operon context, only four of these are MR's. On the basis of genome context, most of the remaining members are expected to be acid sugar dehydratases involved in the catabolism of carbohydrates: the operons that encode them also encode aldolases, dehydrogenases, kinases, and/or mutarotases.

If this expectation is correct, homologues of the acid/base catalysts found in MR that catalyze the 1,1-proton transfer reaction at the α-carbon catalyze dehydration reactions that require proton transfers to/from different carbons, i.e., abstraction of a proton from the 2-carbon to yield the Mg^{2+}-stabilized enediolate intermediate, protonation of the leaving 3-OH group in the vinylogous β-elimination, and, finally, protonation of the 3-carbon of the enol intermediate in the ketonization reaction that yields the product (Scheme 1).

Understanding how the "same" active site responds to the differing structural requirements for dehydration requires that the identities of the substrates for the members of unknown function be established. In this report, we describe the functional assignment of the D-tartrate dehydratase (TarD) function to a member of an orthologous group of proteins in the MR subgroup that, based on sequence alignments, shares the same active site functional groups with MR. We also determined the structure and studied the mechanism of the reaction. Incorporation of the solvent-derived hydrogen into the remaining D-tartrate occurs in competition with dehydration, consistent with our expectation that the TarD-catalyzed reaction is initiated by abstraction of the α-proton by the Lys 184 at the end of the second β-strand. Surprisingly, the incorporation of a solvent-derived hydrogen in the oxaloacetate product, obtained by vinylogous β-elimination of the hydroxide leaving group facilitated by His 322, *occurs in a stereorandom process that is explained by the release of the enol tautomer of oxaloacetate as the product*. Thus, the TarD-catalyzed reaction is a "simple" extension of the two step, MR-catalyzed reaction: initial general base-catalyzed proton abstraction to generate a Mg^{2+}-stabilized enediolate intermediate which is directed to the enol product with the assistance of a general acid catalyst.

MATERIALS AND METHODS

^{1}H NMR spectra were recorded using either a Varian Unity INOVA 750 MHz or a 500NB MHz NMR spectrometer. All reagents were of the highest quality grade commercially available.

Cloning, Expression, and Protein Purification of bll6730, a Protein of Previously Unknown Function. The gene (GI: 27381841) encoding bll6730 was PCR amplified from genomic DNA isolated from *Bradyrhizobium japonicum* (kindly provided by Prof. Kawasaki, Osaka University, Japan) using platinum *Pfx* DNA polymerase (Invitrogen). The PCR reaction (100 μL) contained 1 ng of plasmid DNA, 10 μL of 10× *Pfx* amplification buffer, 1 mM $MgSO_4$, 0.4 mM dNTP, 40 pmol of each primer (forward primer 5′-GAAAGTTGAGACCATATGTCCGTCCGCATC-3′ and reverse primer 5′-CGGCGTGGGGATCCTTACTCCGCCAGC-3′), and 5 units of platinum *Pfx* DNA polymerase. The gene was amplified using a PTC-200 gradient thermal cycler (MJ Research) with the following parameters: 94 °C for 2 min, followed by 40 cycles of 94 °C for 1 min, a gradient temperature range of 45−60 °C for 1 min and 15 s, 68 °C for 2 min, and a final extension of 68 °C for 10 min. The amplified gene was cloned into a modified pET-15b (Novagen) vector in which the N-terminal His tag contains 10 instead of the usual 6 His residues.

The protein was expressed in *Escherichia coli* strain BL21-(DE3). Transformed cells were grown at 37 °C in LB broth (supplemented with 100 μg/mL ampicillin) for 48 h and harvested by centrifugation. No IPTG was added to induce protein expression. The cells were resuspended in binding buffer (5 mM imidazole, 0.5 M NaCl, 20 mM Tris-HCl, pH 7.9, and 5 mM $MgCl_2$) and lysed by sonication. The lysate was cleared by centrifugation, and the His-tagged protein was purified using a column of chelating Sepharose Fast Flow (Amersham Biosciences) charged with Ni^{2+}. Cell lysate was applied to the column in binding buffer, washed with 15% elute buffer (1 M imidazole, 0.5 M NaCl, 20 mM Tris-HCl, pH 7.9, and 5 mM $MgCl_2$)−85% wash buffer (60 mM imidazole, 0.5 M NaCl, 20 mM Tris-HCl, pH 7.9, and 5 mM $MgCl_2$), and eluted with 50% binding buffer−50% strip buffer (100 mM EDTA, 0.5 M NaCl, 20 mM Tris-HCl, pH 7.9, and 5 mM $MgCl_2$). The N-terminal His tag was removed with thrombin (Amersham Biosciences) according to the manufacturer's instructions, and the proteins were purified to homogeneity on a Q-Sepharose high-performance column (Amersham Biosciences) equilibrated with binding buffer (25 mM Tris-HCl, pH 7.9, and 5 mM $MgCl_2$) and eluted with a linear gradient of 0−0.5 M elution buffer (1 M NaCl, 25 mM Tris-HCl, pH 7.9, and 5 mM $MgCl_2$).

Site-Directed Mutagenesis and Protein Purification. Site-directed mutants of TarD were constructed using the QuikChange kit (Stratagene), verified by sequencing, expressed in the BL21(DE3) *E. coli* cells, and purified as previously described for wild-type TarD.

Crystallization and Data Collection. All crystals, wild-type TarD liganded with Mg^2, selenomethionine-substituted TarD liganded with Mg^{2+}, wild-type TarD liganded with Mg^{2+} and *meso*-tartrate, and the K184A mutant liganded with Mg^{2+} and D-tartrate, were grown by the hanging drop method at room temperature. The crystallization conditions for the first two samples were the same: 5.6 mg/mL protein in 50

Table 1: Data Collection and Refinement Statistics

				SeMetTarD·Mg		
	wtTarD·Mg	wtTarD·Mg·*meso*-tar	K184A·TarD·Mg·D-tar	edge	peak	remote
data collection						
beamline	NSLS X9A	NSLS X4A	NSLS X4A	NSLS X9A		
wavelength	0.979	0.979	0.979	0.97936	0.97915	0.97166
space group	$C222_1$	$P1$	$P6_122$	$C222_1$		
unit cell parameters						
a, b, c (Å)	95.97, 178.00, 110.51	74.83, 162.54, 168.18	150.99, −, 444.10	96.03, 178.06, 110.58		
α, β, γ (deg)		117.76, 90.03, 90.67				
no. of molecules in a.u.	2	16	4	2		
resolution (Å)	1.86	2.5	2.3	2.5	2.5	2.5
unique reflections	78930	223601	115401	32987	33052	32965
completeness (%)	99.6	92.3	90.7	99.7	99.8	99.5
R_{merge}	0.061	0.088	0.119	0.056	0.049	0.068
refinement						
resolution (Å)	25.0−1.86	25.0−2.5	25−2.3			
R_{cryst}	0.234	0.241	0.209			
R_{free}	0.254	0.265	0.232			
rmsd, bonds (Å)	0.006	0.007	0.006			
rmsd, angles (deg)	1.30	1.34	1.39			
no. of protein atoms	5850	48352	12072			
no. of ligand atoms	0	160	40			
no. of Mg^{2+}	2	16	4			
no. of waters	303	449	466			
PDB ID	1TZZ	2DW7	2DW6			

mM Hepes, pH 7.0, containing 0.1 M NaCl and 5 mM $MgCl_2$; the precipitant was 17% PEG 3350 and 0.1 M Bis-Tris, pH 5.5. For the crystallization of the wild-type TarD·Mg^{2+}·*meso*-tartrate complex the protein solution contained wild-type TarD (7.2 mg/mL) in 50 mM Tris-HCl, pH 7.9, containing 0.1 M NaCl, 5 mM $MgCl_2$, and 40 mM *meso*-tartrate; the precipitant was 16% PEG3350, 0.1 M Bis-Tris, pH 5.5, and 5% acetone. For the crystallization of the K184A TarD·Mg^{2+}·D-tartrate complex the protein solution contained mutant protein (32 mg/mL) in 50 mM Tris-HCl, pH 7.9, containing 0.1 M NaCl, 5 mM $MgCl_2$, and 40 mM D-tartrate; the precipitant was 0.8 M potassium/sodium tartrate, 0.1 M Tris-HCl, pH 8.5, and 0.5% PEG MME 5000. Crystals of wild-type TarD·Mg^{2+} and SeMet TarD·Mg^{2+} appeared in 3−4 days and exhibited diffraction consistent with the space group $C222_1$ with two molecules in the asymmetric unit. Crystals of the wild-type TarD·Mg^{2+}·*meso*-tartrate complex appeared in 8−9 days and exhibited diffraction consistent with the space group $P1$ with 16 molecules of ternary complex in the asymmetric unit. Crystals of K184A TarD·Mg^{2+}·D-tartrate appeared in 2 weeks and exhibited diffraction consistent with the space group $P6_122$ with four molecules of the ternary complex in the asymmetric unit. Prior to data collection, crystals of wild-type TarD·Mg^{2+} and SeMet TarD·Mg^{2+} were cryoprotected in mother liquor supplemented with 5 mM $MgCl_2$ and 20% glycerol; crystals of wild-type TarD·Mg^{2+}·*meso*-tartrate were cryoprotected in mother liquor supplemented with 5 mM $MgCl_2$, 40 mM *meso*-tartrate, and 30% glycerol; and crystals of K184A TarD·Mg^{2+}·D-tartrate were cryoprotected in mother liquor supplemented with 5 mM $MgCl_2$, 40 mM D-tartrate, and 30% glycerol. After ∼10 s of incubation in cryoprotectant solution all crystals were flash cooled in a nitrogen stream. Three wavelength MAD data for SeMet TarD were collected to 2.5 Å resolution at the NSLS X9A beamline (Brookhaven National Laboratory) on a MarCCD-165 detector. Native data for wild-type TarD to 1.86 Å were collected under the same experimental conditions. Data for the wild-type TarD·Mg^{2+}·*meso*-tartrate ternary complex (2.5 Å resolution) and the K184A TarD·Mg^{2+}·D-tartrate ternary complex (2.3 Å) were collected at the NSLS X4A beamline on an ADSC CCD detector. Data were integrated and scaled with the programs DENZO and SCALEPACK (*11*). Data collection statistics are given in Table 1.

Structure Determination and Refinement. Initial attempts to determine the structure of the wild-type TarD by molecular replacement using other members of enolase superfamily as a search model were unsuccessful. The structure of SeMet TarD was solved by multiple anomalous dispersion (MAD) with the program SOLVE (*12*), which identified 28 out of 30 expected selenium sites. These heavy atom sites were used to calculate initial phases that were improved by solvent flattening and NCS averaging with the program RESOLVE (*13*), yielding an interpretable map for both monomers in the asymmetric unit. Iterative cycles of manual rebuilding with TOM (*14*) and refinement with CNS resulted in a model with $R_{cryst} = 0.249$ and $R_{free} = 0.275$ at 2.5 Å resolution. This model was subsequently refined at 1.86 Å for wild-type TarD with $R_{cryst} = 0.234$ and $R_{free} = 0.254$. The two wild-type TarD molecules in the asymmetric unit form a tight dimer, typical of members of the enolase superfamily. The Mg^{2+} ions were clearly visible in the electron density maps of wild-type TarD for both monomers and were coordinated by Asp 213, Glu 239, Glu 265, and three water molecules. The chain segments composed of residues 18−26 from the flexible 20's loops in both monomers exhibited weak density and were not included in the final model of wild-type TarD. The structure of the wild-type TarD·Mg^{2+}·*meso*-tartrate ternary complex was solved by molecular replacement with the program EPMR, using the wild-type TarD dimer as the search model. The bound *meso*-tartrate and Mg^{2+} were clearly visible in electron density maps for all eight dimers in the asymmetric unit. Several cycles of refinement with the inclusion of water molecules, Mg^{2+}, and inhibitor in the final cycles resulted in a final model with $R_{cryst} = 0.241$ and $R_{free} = 0.265$. All residues of the protein chain are well-

defined and are included in the final model. The structure of the K184A TarD·Mg^{2+}·D-tartrate ternary complex was solved by molecular replacement with the program EPMR, also using the wild-type TarD dimer as the search model. The bound ligands and Mg^{2+} were readily identified in the active sites of the two dimers in the asymmetric unit. Iterative cycles of automatic rebuilding with ARP, manual rebuilding with TOM, and refinement with CNS resulted in a final model with $R_{cryst} = 0.209$ and $R_{free} = 0.232$. The 20's loops that close the active sites are stabilized in the presence of bound D-tartrate in all four monomers; all residues of the protein chains are well-defined and are included in the final model. Final refinement statistics are given in Table 1.

Assignment of D-*Tartrate Dehydratase (TarD) Function to bll6730.* Dehydration of mono- and dicarboxylate acid sugars by the enzyme was monitored after 16 h by end-point detection of the semicarbazone product at 250 nm. The dehydration by TarD was performed at 30 °C in 50 mM Tris-HCl (pH 8.0), containing 10 mM $MgCl_2$, 10 mM acid sugar, and 1 μM enzyme. Acid sugars used include D-, L-, and *meso*-tartrate; xylarate; D- and L-arabinarate; ribarate; allarate; D- and L-altrarate; galactarate; D- and L-glucarate; L-idarate; D- and L-mannarate; D- and L-ribonate; D- and L-arabinonate; D- and L-xylonate; D- and L-lyxonate; D- and L-allonate; D- and L-altronate; D- and L-gluconate; D- and L-mannonate; D- and L-gulonate; D- and L-idonate; D- and L-galactonate; D- and L-talonate; D- and L-fuconate; L-rhamnonate; D-galacturonate; and D-glucuronate (*9*).

Kinetic Assay of D-*Tartrate Dehydratase.* TarD activity was assayed by a continuous coupled spectrophotometric assay, using malate dehydrogenase to reduce the oxaloacetate product to L-malate and quantitating the oxidation of NADH or decrease of absorbance at 340 nm. The assay (1 mL at 25 °C) contained D-tartrate (0.02−10 mM), 50 mM K^+Hepes (pH 7.5), 10 mM $MgCl_2$, 0.16 mM NADH, and 10 units of L-malate dehydrogenase (MDH).

Synthesis of L-*[3(R)-^{2}H]-Malate*. L-[3(*R*)-^{2}H]-Malate was prepared by reacting fumarate and fumarase in D_2O buffer. The reaction mixture contained 50 mM Tris-DCl (pD 7.5), 5 mM fumarate, and 20 units of fumarase. Fumarase was exchanged into D_2O buffer using an Amicon (10000 Da) stirred ultrafiltration cell.

Synthesis of [4(S)-^{2}H]-NADH. [4(*S*)-^{2}H]-NADH was prepared according to the method described by Ottolina et al. (*15*). The reaction mixture (6 mL) contained 50 mM sodium bicarbonate (pH 7.5), 30 mM D-[1-^{2}H]-glucose, 15 mM NAD^+, and 35 units of glucose dehydrogenase. The reaction mixture was incubated at 25 °C for 5 h, and the course of NAD reduction was monitored at 340 nm. The mixture was diluted with water to 15 mL and purified by elution from a column of DEAE-Sepharose Fast Flow (HCO_3^- form) with a gradient of ammonium bicarbonate. Fractions containing [4(*S*)-^{2}H]-NADH were pooled and lyophilized. The stereochemistry and isotopic purity of [4(*S*)-^{2}H]-NADH were determined by ^{1}H NMR spectroscopy.

TarD-Catalyzed Exchange of the α*-Proton of* D-*Tartrate.* D-Tartrate was incubated with wild-type or mutant TarD's in buffered D_2O at 20 °C, and ^{1}H NMR spectra were recorded. A typical reaction contained 5 mM D-tartrate, 50 mM Tris-DCl (pD 7.5), and 0.5 unit of wild-type TarD (or increased amounts of mutant enzymes). Mg^{2+} was omitted from the reaction to minimize nonenzymatic decarboxylation of oxaloacetate.

Stereochemical Course of D-*Tartrate Dehydration.* D-Tartrate was dehydrated in a D_2O-containing buffer at 20 °C, with ^{1}H NMR spectra recorded as a function of time after initiation of the reaction. To determine the stereochemical course of dehydration, MDH was used to reduce the oxaloacetate product to L-malate; due to overlapping ^{1}H chemical shifts of the 3(*R*)-H of L-malate and the 4(*S*)-H of the dihydropyridine ring of NADH, and the fortuitous stereospecificity of MDH for the 4(*R*)-H of NADH, [4(*S*)-^{2}H]-NADH was used in the reductive trapping of the oxaloacetate dehydration product. A typical reaction contained 2.5 mM D-tartrate, 5 mM [4(*S*)-^{2}H]-NADH, 50 mM Tris-DCl (pD 7.5), 25 units of MDH, and 1 unit of wild-type TarD (or increased amounts of mutant enzymes).

Observation of the Tautomers of Oxaloacetate by ^{1}H NMR Spectroscopy. D-Tartrate was dehydrated in a D_2O-containing buffer at 20 °C, with ^{1}H NMR spectra recorded as a function of time after initiation of the reaction. For observation of both the enol and keto tautomers of oxaloacetate, the reactions contained 2.5 mM D-tartrate, 10 mM sodium phosphate (pD 7.5), and 1 unit of wild-type TarD. The identity of the resonance associated with the enol tautomer was established in separate experiments in which the reaction mixture also contained 5 mM [4(*S*)-^{2}H]-NADH and 25 units of MDH.

RESULTS AND DISCUSSION

Assignment of D-*Tartrate Dehydratase Function to bll6730 from B. japonicum (GI:27381841).* The protein that is the focus of this report, bll6730 (GI:27381841) from *B. japonicum*, is a member of a group of proteins in the MR subgroup (now numbering 14) thought to be isofunctional on the basis of sequence alignments (>60% identity).[2] However, the genes encoding these proteins do not share the same genomic context, and insufficient operon context is available for any gene to provide sufficient clues to assign function. In some, but not all, cases, the proximal genes encode dicarboxylic acid transporters and/or diacid dehydrogenases, suggesting that the function of the unknown members would be (di)-acid sugar dehydration. The protein from *B. japonicum* was selected for functional assignment simply on the basis of the availability of its genomic DNA in our laboratory; other orthologues were not studied because the structure was solved by the New York Structural Genomics Research Consortium (NYSGXRC) before systematic attempts at the functional assignment were initiated.

Due to the lack of specific information obtained from the examination of orthologous operon contexts, we used a screening strategy to identify the substrate for bll6730. A

[2] GI:27381841, *Bradyrhizobium japonicum* USDA 110; GI:78699728, *Bradyrhizobium* sp. BTAi1; GI:83375237, *Rhodobacter sphaeroides* ATCC 17029; GI:77465386, *Rhodobacter sphaeroides* 2.4.1; GI:69279803, *Mesorhizobium* sp. BNC1; GI:75433304, *Actinobacillus succinogenes* 130Z; GI:83951719, *Roseovarius nubinhibens* ISM; GI:89899652, *Rhodoferax ferrireducens* DSM 15236; GI:84715239, *Polaromonas naphthalenivorans* CJ2; GI:91782474, *Burkholderia xenovorans* LB400; GI:74015177, *Burkholderia ambifaria* AMMD; GI:91788958, *Polaromonas* sp. JS666; GI:28871205, *Pseudomonas syringae pv.* tomato *str.* DC3000; GI:77458999, *Pseudomonas fluorescens* PfO-1.

Table 2: Kinetic Parameters of TarD

	k_{cat} (s^{-1})	K_M (mM)	k_{cat}/K_M ($M^{-1}\,s^{-1}$)
wild type	7.3 ± 0.1	0.086 ± 0.007	8.5×10^4
K184R	$(5.8 \pm 0.5) \times 10^{-3}$	0.035 ± 0.016	1.7×10^2
K184A	~0		~0
H322N	$(6.9 \pm 0.4) \times 10^{-3}$	0.048 ± 0.019	1.4×10^2
H322Q	$(1.9 \pm 0.4) \times 10^{-3}$	7.7 ± 5.5	2.5×10^{-1}
H322A	$(2.7 \pm 0.2) \times 10^{-3}$	6.2 ± 2.5	4.4×10^{-1}
K102M	~0		~0
K102A	~0		~0

Scheme 2

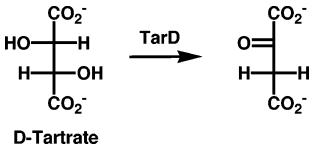

library of 46 mono- and diacid sugars and uronic acids was used to identify possible substrates (*9*). We screened for dehydratase activity by reacting the enzyme−substrate mixtures with the semicarbazide reagent and detecting any semicarbazone product by UV spectroscopy. Under the conditions described in the Materials and Methods section, only D-tartrate was completely dehydrated by bll6730; no other acid sugar resulted in detectable turnover (<1%; results not shown).

We also investigated possible tartrate epimerase activity by ^{1}H NMR spectroscopy in D_2O. *meso*-Tartrate would necessarily be the substrate/product of epimerization; no time-dependent exchange/loss of the ^{1}H NMR resonance of *meso*-tartrate was observed (data not shown).

The product initially was identified as oxaloacetate using L-malate dehydrogenase (MDH) in a coupled-enzyme spectrophotometric assay; in the absence of exogenous Mg^{2+}, no pyruvate could be detected using L-lactate dehydrogenase (data not shown). The values of the kinetic constants are listed in Table 2. With these values for the kinetic constants, which are comparable to those measured for GalD (*8*), GlucD (*16*), and FucD (*9*), we consider D-tartrate to be the physiological substrate of bll6730, so we assign the function as D-tartrate dehydratase (TarD; Scheme 2).

On the basis of sequence homology (conservation of residues in the loops in the N-terminal capping domain that determined substrate specificity), we assume that the TarD function is shared by the other members of the presumed orthologous group.[2]

Structure of TarD. Like FucD, but in contrast to the octameric MR, TarD is an α_2 homodimer, in which the monomer exhibits two distinct domains. The $(\beta/\alpha)_7\beta$-barrel domain containing the metal ion ligands and acid/base groups and the capping domain formed the extra barrel N- and C-terminal segments of the polypeptide forming the binding pocket for the substrate. As previously observed for MR and FucD, each active site is at the interface between two symmetry-related polypeptides (Figure 1), so the octameric structure is best described as a tetramer of dimers.

Structures were determined for three forms of the enzyme: wild type liganded only with Mg^{2+}, wild type liganded with Mg^{2+} and *meso*-tartrate (a competitive inhibitor; $K_i = 20\ \mu M$), and the K184A mutant (active site base; vide infra) liganded with Mg^{2+} and D-tartrate (the substrate).

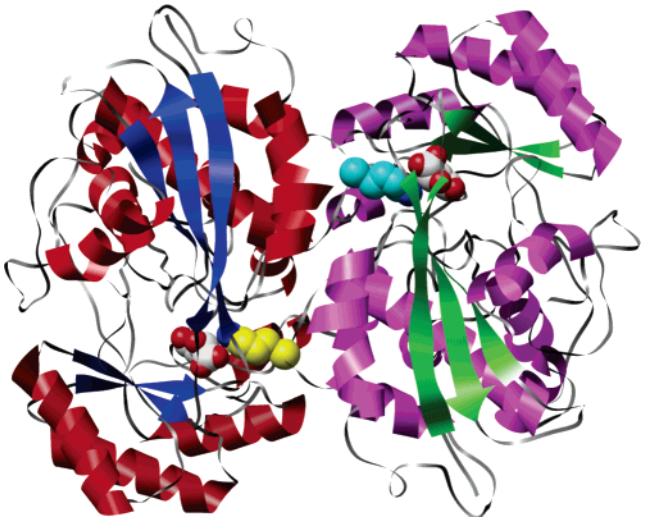

FIGURE 1: The dimer of TarD in the structure of wild-type TarD complexed with *meso*-tartrate (white). The α-helices and β-strands in one polypeptide are colored red and blue, respectively; in the second polypeptide these are colored magenta and green, respectively. Lys 102 from the second polypeptide, colored yellow, participates in the active site of the first polypeptide; Lys 102 from the first polypeptide, colored cyan, participates in the active site of the second polypeptide.

The D-tartrate substrate has the 2*S*,3*S* configuration; the inert *meso*-tartrate inhibitor has the 2*S*,3*R* configuration.

The active site of the complex of wild-type TarD with Mg^{2+} and *meso*-tartrate is shown in Figure 2A. As expected, the Mg^{2+} is coordinated to Asp 213, Glu 239, and Glu 265, located at the ends of the third, fourth, and fifth β-strands in the barrel domain. One carboxylate oxygen of the inhibitor is coordinated to the Mg^{2+} as well as hydrogen bonded to the ϵ-ammonium group of Lys 182 located at the end of the second β-strand. The second carboxylate oxygen is hydrogen bonded to Glu 341, located at the end of the eighth β-strand. This coordination of the essential Mg^{2+} is analogous to that observed in the active site of MR and FucD. The distal carboxylate group of the inhibitor is hydrogen bonded to both Asn 21 in the 20's loop in the capping domain and Lys 102 in the capping domain of the symmetry-related polypeptide in the dimer. In MR, a Val at a homologous position in the capping domain of the symmetry-related polypeptide completes the hydrophobic cavity of the active site.

The proton of the 2*S*-carbon of the inhibitor points toward Lys 184 at the end of the second β-strand in the KxK motif. On the basis of this location, Lys 184 is positioned to function as the general acid catalyst to catalyze abstraction of the 2-proton, although the 2*S*-proton *meso*-tartrate is inert to proton abstraction as judged by the lack of exchange of this proton with solvent (vide supra). His 322, of the His 322-Asp 292 dyad at the ends of the seventh and sixth β-strands, respectively, is located on the opposite face of the active site.

The 3(*R*)-OH group of the inhibitor is hydrogen bonded to Asn 55 in the capping domain, Tyr 343 at the end of the eighth β-strand, and His 322. As illustrated in Figure 2A, both the structure of *meso*-tartrate and the geometry of the hydrogen-bonding network enforce the 3-OH group to be in the plane of the enolate anion intermediate generated by abstraction of the α-proton, thereby preventing its departure in a vinylogous β-elimination reaction.

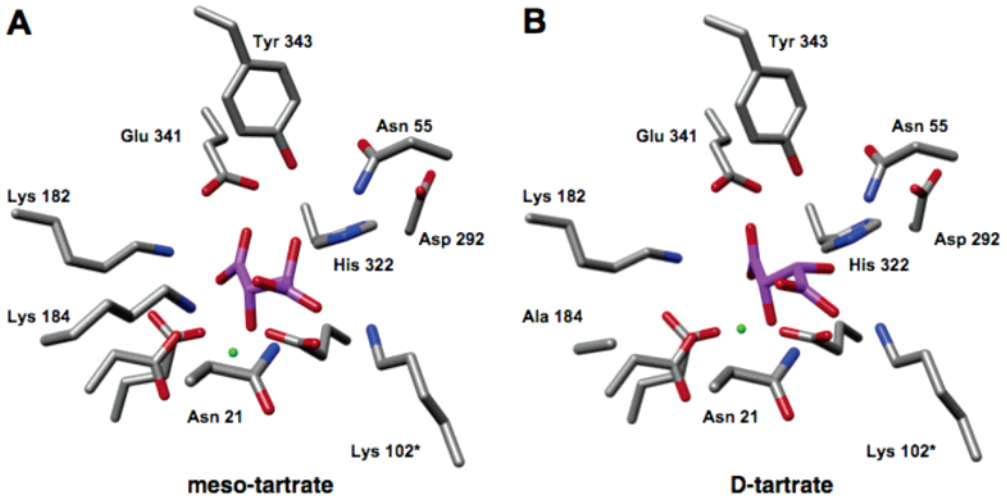

FIGURE 2: Panel A: The active site of wild-type TarD complexed with the competitive inhibitor *meso*-tartrate (purple). Panel B: The active site of the K184A mutant of TarD complexed with the substrate D-tartrate (purple).

The active site of the complex of the K184A mutant of TarD with Mg^{2+} and D-tartrate (the substrate for wild-type TarD) is shown in Figure 2B. The essential differences between this complex and that of wild-type TarD with *meso*-tartrate are (1) the absence of the side chain of putative general basic Lys 184 and (2) the loss of the hydrogen bond between the 3-OH group of the ligand and Tyr 343. As illustrated in Figure 2B, both the structure of D-tartrate and the geometry of the hydrogen-bonding network enforce the 3-OH group to be orthogonal to the plane of the enolate anion intermediate generated by abstraction of the α-proton, thereby allowing its departure in a vinylogous *β*-elimination reaction assisted by general acid catalysis by His 322. A similar disposition of the 3-OH leaving group of L-fuconate was observed in the catalytically inactive K220A mutant of FucD (*9*).

Thus, on the basis of the structures of these complexes, we propose that the TarD-catalyzed reaction involves initial abstraction of the 2-proton of D-tartrate to generate an enolate anion intermediate stabilized by enhanced electrostatic interactions with the Mg^{2+} and enhanced hydrogen bonding with Glu 341 followed by general acid-catalyzed departure of the orthogonal 3-OH group by His 322. The remaining sections of this paper describe experimental examination of this hypothesis.

Kinetic Properties of Mutants of Active Site Residues. We constructed the mutants listed in Table 2 so that their kinetic importance in the TarD-catalyzed reaction could be evaluated. The values of the kinetic constants are also included in Table 2.

The values of the kinetic constants are consistent with Lys 184 functioning as the *S*-specific base that initiates the reaction (vide infra); e.g., the activity was reduced by the K184R mutant and eliminated by the K184A mutant. The substitutions for His 322 retained low, but measurable, levels of activity, suggesting that the abstraction of the α-proton can be catalyzed and that the vinylogous *β*-elimination of the hydroxyl leaving group can proceed but at a significantly decreased rate in the absence of a general acid catalyst. The presence of Lys 102 in the active site suggests that it might be able to provide a proton for *β*-elimination in the absence of His 322; however, the K102M and K102A mutants have no detectable activity, suggesting perturbations in the structure of the active site and/or significantly diminished affinity for the dianionic substrate.

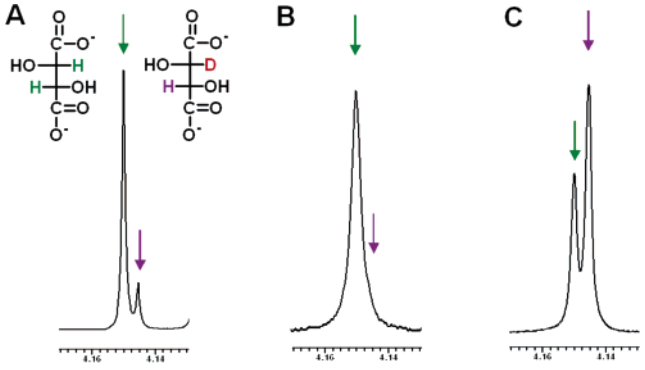

FIGURE 3: Representative ^1H NMR spectrum of D-tartrate after incubation with (A) wild-type TarD, (B) K184R, and (C) H322N.

Mechanism of the TarD-Catalyzed Reaction: Exchange of the α-Proton of D-Tartrate Occurs in Competition with Dehydration. We examined the progress of the wild-type TarD-catalyzed reaction using ^1H NMR spectroscopy in Tris-HCl-buffered D_2O as solvent. We observed a decrease in the intensity associated with the protons of D-tartrate, but no resonances associated with oxaloacetate were visible due to rapid exchange of their protons with the D_2O solvent.

As the resonance associated with D-tartrate decreased in intensity, we observed the transient formation of an upfield-shifted resonance associated with D-[$^2H_1$]-tartrate (Figure 3A). The appearance of this resonance can be explained by the abstraction of the α-proton of D-tartrate by a polyprotic active site base to generate the Mg^{2+}-stabilized enediolate intermediate which can partition between vinylogous *β*-elimination to accomplish dehydration to the enol of oxaloacetate and deuteriation by the conjugate acid of the polyprotic base to yield D-[$^2H_1$]-tartrate (Scheme 3). Subsequent binding of the pseudosymmetrical D-[$^2H_1$]-tartrate to TarD such that the proton rather than the deuteron is positioned for abstraction by Lys 184 is expected to yield both dehydration and the spectroscopically invisible D-[$^2H_2$]-tartrate. Of course, the hydron abstraction steps from D-tartrate, D-[$^2H_1$]-tartrate, and D-[$^2H_2$]-tartrate will be accompanied by solvent and substrate (D-[$^2H_1$]- and D-[$^2H_2$]-tartrate) kinetic isotope effects.

The exchange of the α-proton of D-tartrate with solvent deuterium catalyzed by TarD is reminiscent of the observa-

Scheme 3

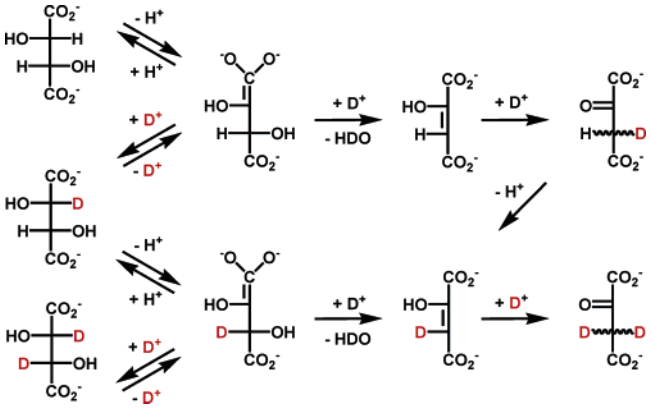

tion that the α-proton of (*S*)-mandelate, but not (*R*)-mandelate, is exchanged with solvent deuterium in the MR-catalyzed reaction (*17*). However, in the case of the TarD-catalyzed reaction, the structure/symmetry of D-tartrate allows the exchange reaction to be observed directly by ^{1}H NMR spectroscopy. In the MR-catalyzed reaction, the incorporation of solvent deuterium into the (*S*)-mandelate substrate pool was quantitated by derivitization with a chiral reagent followed by GC-MS analyses to quantitate the incorporation

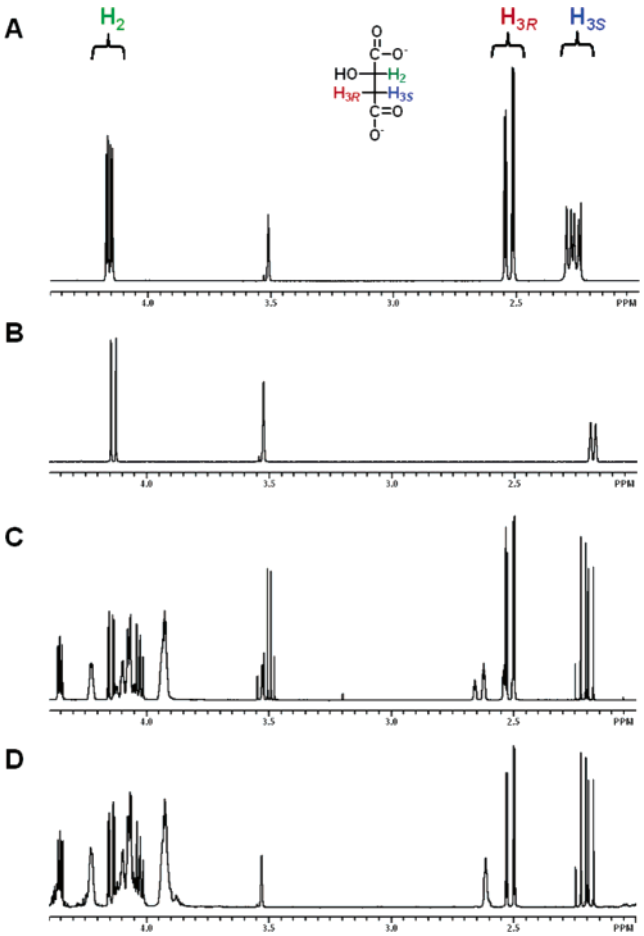

FIGURE 4: (A) ^{1}H NMR spectrum of L-malate showing the assignments of the prochiral protons of C3 of L-malate. (B) ^{1}H NMR spectrum of L-[3(*R*)-^{2}H]-malate. (C) ^{1}H NMR spectrum of a mixture of NADH and L-malate showing the overlap of the resonances associated with the 3-*pro*-*R* proton of L-malate and the 4-*pro*-*S* proton of NADH. (D) ^{1}H NMR spectrum of a mixture of [4(*S*)-^{2}H]-NADH and L-malate.

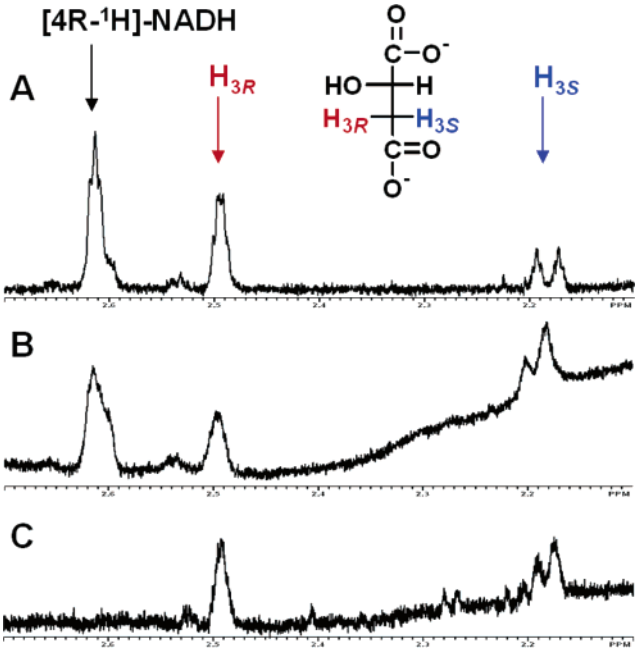

FIGURE 5: ^{1}H NMR spectra of L-malate obtained after incubation of 2.5 mM D-tartrate, 5 mM [4(*S*)-^{2}H]-NADH, and L-malate dehydrogenase with wild-type TarD (panel A) and K184R (panel B). Because of enhanced exchange of the D-tartrate substrate with solvent deuterium, 25 mM D-tartrate was used in analogous experiments with H322N (panel C).

of solvent deuterium. For MR, the exchange reaction was explained by the polyprotic Lys 166 acting as the *S*-specific base in the MR-catalyzed reaction, with the enediolate intermediate partitioning between protonation on the opposite face by the conjugate acid of His 297 to yield (*R*)-mandelate and deuteriation by the conjugate acid of Lys 166 to yield deuteriated (*S*)-mandelate. In support of this mechanism, the N297N mutant of MR was active as an (*S*)-mandelate "exchangease" but inactive as a racemase (*18*).

Thus, the general base in the TarD-catalyzed reaction is Lys 184, the homologous residue of Lys 166 in MR, which would be dideuteriated in the enzyme·D-tartrate complex and, after proton abstraction and rotation about the $C_\epsilon-N_\epsilon$ bond, be properly positioned to competitively deliver a deuteron to the intermediate to generate the observed D-[$^2H_1$]-tartrate.

We also examined the ability of the active site mutants to catalyze the incorporation of solvent deuterium into the remaining D-tartrate. In the case of potentially torsiosymmetric K184R substitution, which catalyzes slow dehydration, no formation of deuteriated D-tartrate was observed as the D-tartrate was consumed (Figure 3B); presumably, the substitution increases the energy barrier for partitioning of the enediolate intermediate to exchange relative to dehydration. In the case of H322N, which also catalyzes slow dehydration, the amount of D-[$^2H_1$]-tartrate that accumulated exceeded that observed in the course of the reaction catalyzed by wild-type TarD; in this case, the substitution substantially increases the energy barrier for partitioning of the enediolate intermediate to dehydration relative to that for exchange (Figure 3C).

This behavior is consistent with the role of Lys 184 as the general base that initiates the reaction by abstraction of the α-proton and of His 322 as assisting in the vinylogous β-elimination of the 3-hydroxyl group. As expected from

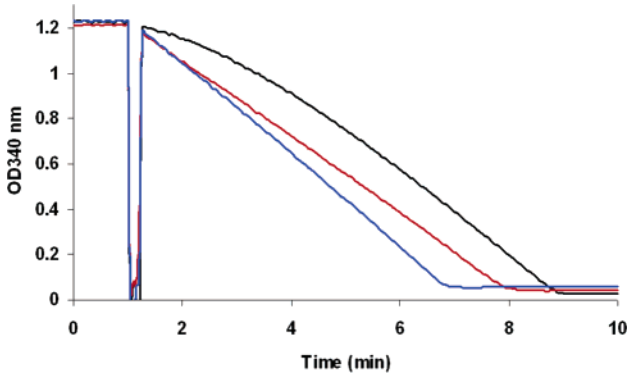

FIGURE 6: Time course for consumption of NADH in the MDH coupled-enzyme assay. The assay was performed in 10 mM sodium phosphate buffer, pH 7.5 (black line); in 10 mM sodium phosphate buffer and 10 mM $MgCl_2$ (red line); and in 50 mM K^+Hepes buffer and 10 mM $MgCl_2$ (blue line).

this proposal, the K184A mutant was devoid of measurable TarD activity, allowing its structure to be determined in the presence of D-tartrate. However, in contrast to the MR-catalyzed reaction in which H297N was devoid of racemase activity, the H322N retained decreased, but measurable, dehydration activity.

Mechanism of the TarD-Catalyzed Reaction: Stereochemical Course of the Dehydration Reaction. We analyzed the stereochemical course of replacement of the 3-OH group with solvent-derived hydrogen so that we could determine the relative orientation of the hydroxyl leaving group and the general acid involved in ketonization of the enol intermediate (formed by vinylogous β-elimination of water) to form the oxaloacetate product (Scheme 1). Because we observed that the protons of the oxaloacetate product exchange rapidly with the D_2O solvent, we conducted the TarD-catalyzed reaction in the presence of a kinetic excess of MDH to trap the keto tautomer of the oxaloacetate product as L-malate.

The protons of the methylene group of L-malate, derived from the methylene group of oxaloacetate in the MDH-catalyzed reaction, appear as an ABX pattern (Figure 4A), with the downfield signals associated with the 3-*pro-R* proton (assigned by comparison with L-[3(*R*)-^{2}H]-malate prepared by the fumarase-catalyzed hydration of fumarate in D_2O) (Figure 4B). We also observed that the 3-*pro-R* proton of L-malate and the 4-*pro-S* proton of NADH have similar chemical shifts (Figure 4C), so we utilized [4(*S*)-^{2}H]-NADH in our stereochemical experiments to allow monitoring of the incorporation of solvent deuterium into the protons of oxaloacetate/L-malate throughout the course of the reaction (Figure 4D).

After completion of the wild-type TarD-catalyzed reaction conducted in the presence of a molar excess of [4(*S*)-^{2}H]-NADH, both L-[3(*S*)-^{2}H]- and L-[3(*R*)-^{2}H]-malate were produced in approximately equimolar amounts (Figure 5A). The stereochemical course of replacement of the 3-OH of D-tartrate by a solvent-derived deuterium to yield [3(*S*)-^{2}H]-oxaloacetate (after trapping, L-[3(*S*)-^{2}H]-malate) is retention of configuration; the [3(*R*)-^{2}H]-oxaloacetate (after trapping, L-[3(*R*)-^{2}H]-malate) is formed with inversion of configuration. Thus, the delivery of a solvent-derived hydrogen to the enol intermediate to yield the keto tautomer of oxaloacetate is stereorandom. This observation contrasts with our earlier reports that solvent-derived hydrogen is incorporated with retention of configuration in the dehydration reactions catalyzed by both GalD and GlucD (*8*) and with inversion of configuration in the reaction catalyzed by L-fuconate dehydratase (*9*). Assuming that the dehydration proceeds with an anti-stereochemical course, based on the importance of both Lys 184 and His 322 in the reaction, the solvent-derived hydrogen leading to inversion of configuration in the loss of the hydroxyl group would be delivered from the side of the active site on which Lys 184 is located; the solvent-derived hydrogen leading to retention of configuration would be delivered from the side of the active site on which His 322 is located.

In either Tris-HCl- or phosphate-buffered D_2O, the sum of the integral of the resonances associated with L-[3(*S*)-^{2}H]- and L-[3(*R*)-^{2}H]-malate is 0.7, measured relative to the decreases in the intensities of the downfield, well-resolved resonances associated with NADH and NAD^+. That this intensity is <1 is explained by the enrichment of the D-tartrate substrate with D-[$^2H_1$]- and D-[$^2H_2$]-tartrate as the reaction proceeds (Scheme 2), so that a fraction of the enol

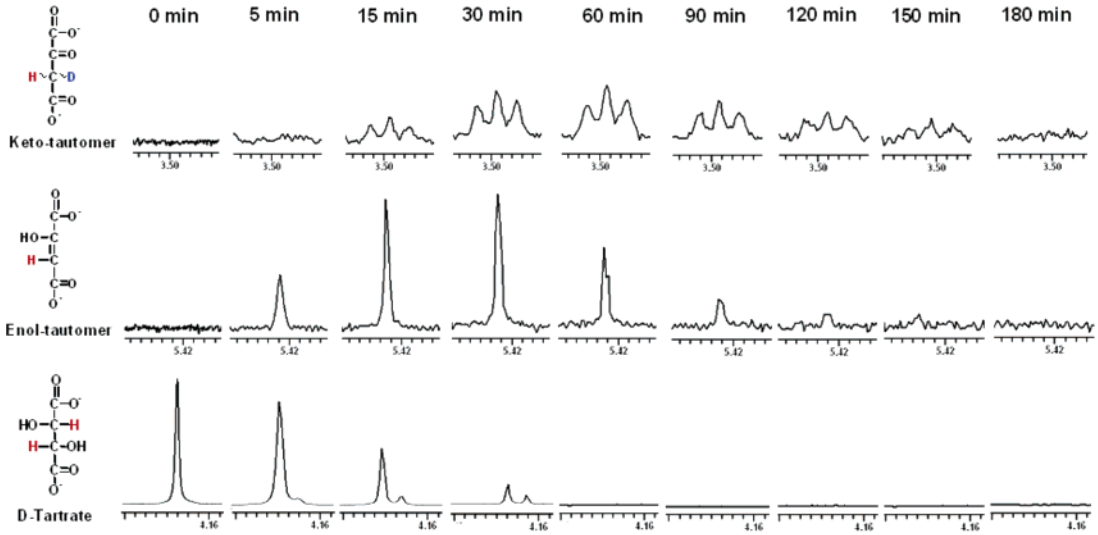

FIGURE 7: ^{1}H NMR spectra of D-tartrate, enol-oxaloacetate, and keto-oxaloacetate obtained as a function of time after addition of 1 unit of TarD to 2.5 mM D-tartrate in 0.8 mL of 10 mM sodium phosphate (pH 7.5). The intensities of the D-tartrate resonances are reduced 20-fold compared to the oxaloacetate resonances.

Scheme 4

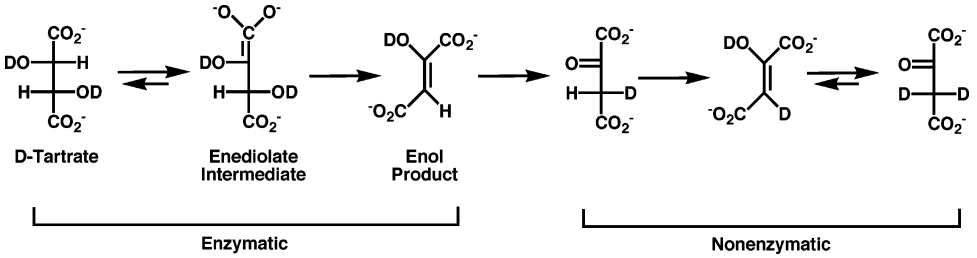

of oxaloacetate resulting from vinylogous β-elimination is deuteriated. After tautomerization in D_2O, the keto tautomer of oxaloacetate which is the substrate for MDH would be dideuteriated, resulting in loss of signal intensity. Loss of protium could result from exchange of the keto tautomer of [$^2H_1$]-oxaloacetate with solvent; however, we observed the intensity of the resonances associated with L-[3(*S*)-^{2}H]- and L-[3(*R*)-^{2}H]-malate to be independent of the amount of MDH used to trap the keto tautomer.

We also examined the stereochemical courses of the reactions catalyzed by the K184R and H322N mutants. In the case of the K184R-catalyzed reaction, L-[3(*S*)-^{2}H]- and L-[3(*R*)-^{2}H]-malate were also produced in equimolar amounts; i.e., the reaction proceeded with equal contributions of pathways accompanied by retention and inversion of configuration (Figure 5B). The sum of the integrals associated with the 3-protons of the oxaloacetate product is 1.0, which is consistent with the observed lack of incorporation of deuterium into the remaining D-tartrate substrate as the dehydration reaction proceeds. Additionally, the quantitative retention of the substrate-derived protium in the trapped L-[3(*S*)-^{2}H]- and L-[3(*R*)-^{2}H]-malates provides additional evidence that the MDH effectively competes with exchange of the keto tautomer of [$^2H_1$]-oxaloacetate with solvent.

The stereochemical course of the H322N-catalyzed reaction could not be studied using the "low", but saturating, concentration of D-tartrate employed in the experiments using wild type and the K184R mutant (2.5 mM). As discussed previously, the H322N-catalyzed reaction is accompanied by more efficient exchange than dehydration, with the consequence that almost all of the oxaloacetate trapped as L-malate was dideuteriated. However, using the same (5 mM; now limiting) concentration of [4(*S*)-^{2}H]-NADH and a 10-fold greater concentration of D-tartrate so that the D-[$^2H_1$]- and D-[$^2H_2$]-tartrate formed by exchange is diluted into a larger reservoir of protiated D-tartrate, we observed that L-[3(*S*)-^{2}H]- and L-[3(*R*)-^{2}H]-malate again were produced in equimolar amounts; i.e., the reaction proceeded with equal contributions of pathways accompanied by retention and inversion of configuration (Figure 5C).

Mechanism of the TarD-Catalyzed Reaction: Observation of the Enol of Oxaloacetate as the Product. That the reactions catalyzed by wild-type TarD and its K184R and H322N mutants are accompanied by stereorandom replacement of the 3-OH group with solvent-derived hydrogen was unexpected. The reactions catalyzed by GalD (*8*), GlucD (*8*), and FucD (*9*) [and those catalyzed by L-fuconate dehydratase (*9*) and both D-mannonate dehydratase and L-rhamnonate dehydratase (J. Rakus and J. A. Gerlt, unpublished observations)] are accompanied by stereospecific replacement of the 3-OH group with solvent-derived hydrogen, providing persuasive evidence that these active sites catalyze the stereospecific tautomerization of the enol intermediate to generate the 2-keto-3-deoxy products (Scheme 1). The "simplest" explanation for the lack of stereospecificity observed for the TarD-catalyzed reaction is that the product is the enol tautomer of oxaloacetate; i.e., the enzyme does not catalyze the ketonization reaction shown in Scheme 1.

Recognizing that amine buffers catalyze tautomerization of carbonyl compounds, including oxaloacetate (*19*−*22*), we performed experiments in phosphate buffer in the absence of exogenous Mg^{2+} to determine which tautomer of oxaloacetate is the product of the TarD-catalyzed reaction. First, we performed the MDH coupled-enzyme assay and observed a pronounced time-dependent increase in activity (lag) that was independent of the amount of MDH present in the assay (Figure 6, black line). This lag was eliminated by including 10 mM $MgCl_2$ in the assay (red line). Also, no lag was observed when the assay was performed in Hepes buffer containing 10 mM $MgCl_2$ (blue line). We attribute the slow attainment of the steady-state rate described by the black line to the nonenzymatic conversion of the enol tautomer product of the TarD-catalyzed reaction to the keto tautomer substrate for the MDH-catalyzed reaction. The time dependence of the observed increase in rate is consistent with that reported by Creighton and co-workers for the nonenzymatic reactions that equilibrate the enol and keto tautomers of oxaloacetate in dilute phosphate buffer at neutral pH (*23*).

We also used ^{1}H NMR spectroscopy to detect the presence of the enol and keto tautomers of oxaloacetate in the TarD-catalyzed reaction.[3] In the absence of MDH (Figure 7), as the D-tartrate is consumed (and, also, competitively undergoes exchange with solvent deuterium), a resonance associated with the enol tautomer of oxaloacetate increases in intensity at 5.43 ppm; this resonance remains until the reservoir of protiated D-tartrate is exhausted. Subsequent to the appearance of this resonance, a resonance associated with the keto tautomer of [$^1H_1$,$^2H_1$]-oxaloacetate appears at 3.5 ppm (a broad triplet because of geminal coupling to the deuterium). The latter resonance decays following that associated with the enol tautomer, as expected if the keto tautomer were derived from the enol tautomer and more exchanges its protium with solvent deuterium via enolization (*23*) (Scheme 3). According to Creighton's measurements, at equilibrium, the enol and keto tautomers of oxaloacetate are present as a 1:10 mixture in aqueous solution, with the enol tautomerizing to the keto about 10-fold faster than the keto tautomerizes

[3] Note that these experiments cannot be performed in the rigorous absence of Mg^{2+} that catalyzes interconversion of the tautomers because the TarD-catalyzed reaction requires Mg^{2+}. The only Mg^{2+} present is that present in the buffer in which the TarD was stored and diluted into the reaction mixture.

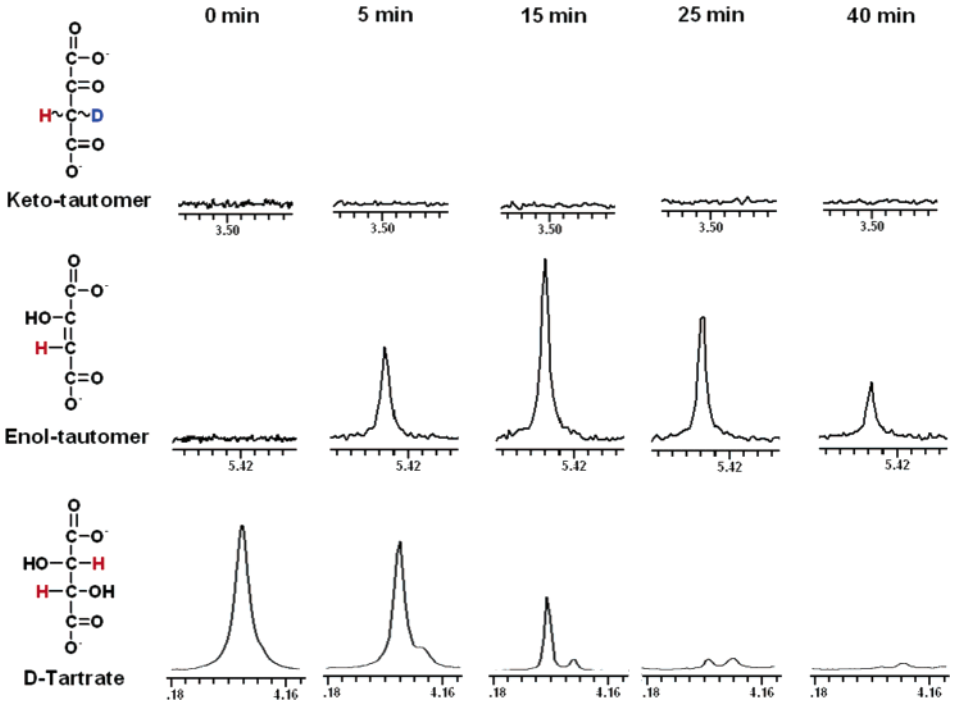

FIGURE 8: ^{1}H NMR spectra of D-tartrate and enol-oxaloacetate obtained as a function of time after addition of 1 unit of TarD to 2.5 mM D-tartrate, 25 units of MDH, and 5 mM [4(*S*)-^{2}H]-NADH in 0.8 mL of 10 mM sodium phosphate (pH 7.5). The intensities of the D-tartrate resonances are reduced 20-fold compared to the oxaloacetate resonances.

to the enol. That the enol tautomer is observed prior to the keto tautomer is persuasive evidence that the enol tautomer of oxaloacetate is the product of the TarD-catalyzed reaction (Scheme 4).

We also used ^{1}H NMR spectroscopy to follow the time course of the TarD-catalyzed reaction in the presence of MDH (Figure 8). The resonance associated with D-tartrate is resolved from those associated with the nucleotides, so we could monitor the consumption of D-tartrate and its exchange with solvent deuterium. We also observed the buildup and decay of the resonance at 5.43 ppm associated with the enol tautomer of oxaloacetate. However, the resonance associated with the keto tautomer of oxaloacetate was not observed in this experiment, because it is trapped as L-malate by the MDH.

Taken together, these observations establish that the enol tautomer of oxaloacetate is the product of the TarD-catalyzed reaction.

Mechanism of the TarD-Catalyzed Reaction. The observations reported in this report provide persuasive evidence that Lys 184 located at the end of the second β-strand is the general base that initiates the reaction by abstraction of the α-proton of the D-tartrate substrate (Figure 9). That the enediolate intermediate partitions much more frequently to D-tartrate with incorporation of solvent deuterium than to dehydration in the H322N-catalyzed reaction is consistent with the latter residue catalyzing the departure of the hydroxyl leaving group. However, in contrast to the inactive H297N mutant of MR, β-elimination of hydroxide can occur in the absence of the conjugate acid of His 322. Taken together, the available data are consistent with the TarD catalyzing an anti-dehydration reaction.

Our experiments establish that TarD releases the enol tautomer of oxaloacetate as the product. That TarD does not catalyze ketonization of this species is in contrast to our

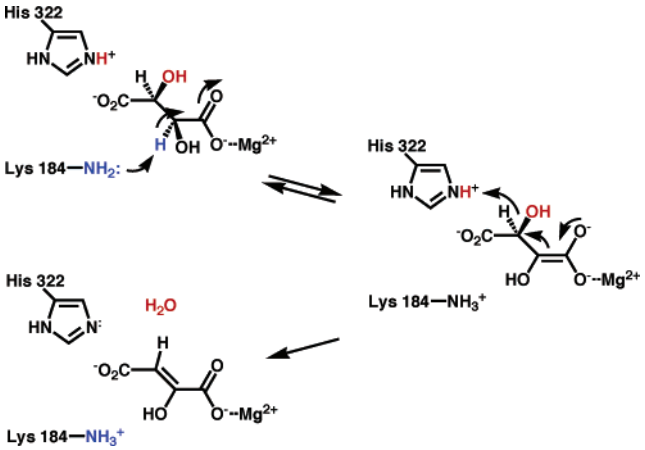

FIGURE 9: Proposed mechanism of the TarD-catalyzed reaction.

observations on the reactions catalyzed by other acid sugar dehydratases that are members of the enolase superfamily. However, unlike the more stable keto tautomers of the dehydrated products obtained from D-glucarate, D-galactonate, and L-fuconate, the enol and keto tautomers of oxaloacetate are nearly equivalent in energy (because of conjugation of the enol tautomer) and, also, are expected to rapidly equilibrate within bacterial cells. Thus, little evolutionary pressure for catalysis of the ketonization reaction may have occurred in the evolution of the TarD function.

Presumably, TarD functions in catabolic pathways in those species in which it has been discovered by genome sequencing projects. Although the genome contexts do not provide sufficient information to deduce the identities of those pathways, the likely fates of the oxaloacetate are either decarboxylation to produce pyruvate or reduction to produce L-malate. In either case, the keto tautomer would be the substrate for subsequent enzyme in the pathway. However, that tautomerization is catalyzed by Mg^{2+} as well as by a

variety of buffers suggests that the in vivo nonenzymatic formation of the keto tautomer is facile.

Summary. A new function, TarD, has been assigned to a member of the MR subgroup of the enolase superfamily, bll6730 from *B. japonicum* (GI:27381841), by screening a library of mono- and diacid sugars. As expected on the basis of the sequence alignment, both the bidomain structure and the active site geometry are similar to those previously described for MR and FucD. Mechanistic experiments implicate Lys 184 located at the end of the second β-strand and the His 322-Asp 292 dyad located at the ends of the seventh and sixth β-strands, respectively, as the general base and general acid catalysts, respectively, in an anti-dehydration reaction. Unexpectedly, the enol tautomer of oxaloacetate is the product of the reaction. TarD appears to provide a link between the 1,1-proton transfer reaction catalyzed by mandelate racemase and the dehydration reactions catalyzed by other acid sugar dehydratases that generate the keto tautomers of their products.

REFERENCES

1. Gerlt, J. A., and Babbitt, P. C. (2001) Divergent evolution of enzymatic function: Mechanistically diverse superfamilies and functionally distinct suprafamilies, *Annu. Rev. Biochem. 70*, 209−246.
2. Gerlt, J. A., and Raushel, F. M. (2003) Evolution of function in (beta/alpha)(8)-barrel enzymes, *Curr. Opin. Chem. Biol. 7*, 252−264.
3. Gerlt, J. A., Babbitt, P. C., and Rayment, I. (2005) Divergent evolution in the enolase superfamily: the interplay of mechanism and specificity, *Arch. Biochem. Biophys. 433*, 59−70.
4. Babbitt, P. C., Hasson, M. S., Wedekind, J. E., Palmer, D. R., Barrett, W. C., Reed, G. H., Rayment, I., Ringe, D., Kenyon, G. L., and Gerlt, J. A. (1996) The enolase superfamily: a general strategy for enzyme-catalyzed abstraction of the alpha-protons of carboxylic acids, *Biochemistry 35*, 16489−16501.
5. Schmidt, D. M., Hubbard, B. K., and Gerlt, J. A. (2001) Evolution of enzymatic activities in the enolase superfamily: Functional assignment of unknown proteins in *Bacillus subtilis* and *Escherichia coli* as L-Ala-D/L-Glu epimerases, *Biochemistry 40*, 15707−15715.
6. Sakai, A., Xiang, D. F., Xu, C., Song, L., Yew, W. S., Raushel, F. M., and Gerlt, J. A. (2006) Evolution of enzymatic activities in the enolase superfamily: *N*-succinylamino acid racemase and a new pathway for the irreversible conversion of D- to L-amino acids, *Biochemistry 45*, 4455−4462.
7. Babbitt, P. C., Mrachko, G. T., Hasson, M. S., Huisman, G. W., Kolter, R., Ringe, D., Petsko, G. A., Kenyon, G. L., and Gerlt, J. A. (1995) A functionally diverse enzyme superfamily that abstracts the alpha protons of carboxylic acids, *Science 267*, 1159−1161.
8. Wieczorek, S. W., Kalivoda, K. A., Clifton, J. G., Ringe, D., Petsko, G. A., and Gerlt, J. A. (1999) Evolution of enzymatic activities in the enolase superfamily: Identification of a "new" general acid catalyst in the active site of D-galactonate dehydratase from *Escherichia coli*, *J. Am. Chem. Soc. 121*, 4540−4541.
9. Yew, W. S., Fedorov, A. A., Fedorov, E. V., Rakus, J. F., Pierce, R. W., Almo, S. C., and Gerlt, J. A. (2006) Evolution of enzymatic activities in the enolase superfamily: L-Fuconate dehydratase from *Xanthomonas campestris*, *Biochemistry 45*, 14582−14597.
10. Kenyon, G. L., Gerlt, J. A., Petsko, G. A., and Kozarich, J. W. (1995) Mandelate racemase: Structure−function studies of a pseudosymmetric enzyme, *Acc. Chem. Res. 28*, 178−186.
11. Otwinowski, Z., and Minor, W. (1997) Processing of X-ray diffraction data collected in oscillation mode, in *Methods in Enzymology* (Carter, C. W. J., Sweet, R. M., Abelson, J. N., and Simon, M. I., Eds.) pp 307−326, Academic Press, New York.
12. Terwilliger, T. C., and Berendzen, J. (1999) Automated MAD and MIR structure solution, *Acta Crystallogr., Sect. D: Biol. Crystallogr. 55*, 849−861.
13. Brunger, A. T., Adams, P. D., Clore, G. M., DeLAno, W. L., Gros, P., Grosse-Kunstleve, R. W., Jiang, J. S., Kuszewski, J., Nilges, M., Pannu, N. S., Read, R. J., Rice, L. M., Simonson, T., and Warren, G. L. (1998) Crystallography & NMR system: A new software suite for macromolecular structure determination, *Acta Crystallogr. D54*.
14. Jones, A. T. (1985) Interactive computer graphics: FRODO, *Methods Enzymol. 115*, 157−171.
15. Ottolina, G., Riva, S., Carrea, G., Danieli, B., and Buckmann, A. F. (1989) Enzymatic synthesis of [4R-2H]NAD (P)H and [4S-2H]NAD(P)H and determination of the stereospecificity of 7 alpha- and 12 alpha hydroxysteroid dehydrogenase, *Biochim. Biophys. Acta 998*, 173−178.
16. Hubbard, B. K., Koch, M., Palmer, D. R., Babbitt, P. C., and Gerlt, J. A. (1998) Evolution of enzymatic activities in the enolase superfamily: characterization of the D-glucarate/galactarate catabolic pathway in *Escherichia coli*, *Biochemistry 37*, 14369−14375.
17. Powers, V. M., Koo, C. W., Kenyon, G. L., Gerlt, J. A., and Kozarich, J. W. (1991) Mechanism of the reaction catalyzed by mandelate racemase. 1. Chemical and kinetic evidence for a two-base mechanism, *Biochemistry 30*, 9255−9263.
18. Landro, J. A., Kallarakal, A. T., Ransom, S. C., Gerlt, J. A., Kozarich, J. W., Neidhart, D. J., and Kenyon, G. L. (1991) Mechanism of the reaction catalyzed by mandelate racemase. 3. Asymmetry in reactions catalyzed by the H297N mutant, *Biochemistry 30*, 9274−9281.
19. Bruice, P. Y. (1983) Formation of a carbinolamine intermediate in the tertiary amine catalyzed enolization of oxaloacetic acid. An alternative mechanism for enolization, *J. Am. Chem. Soc. 105*, 4982−4996.
20. Bruice, P. Y. (1989) Catalysis of the enolization of oxaloacetic acid by primary and secondary amines via a carbinolamine intermediate, *J. Am. Chem. Soc. 111*, 962−970.
21. Bruice, P. Y., and Bruice, T. C. (1978) Lack of concertedness in the catalysis of the enolization of oxaloacetic acid by general acids and bases. Formation of a carbinolamine intermediate in the tertiary amine catalyzed enolization reaction, *J. Am. Chem. Soc. 100*, 4793−4801.
22. Emly, M., and Leussing, D. L. (1981) Dehydration and enolization of oxalacetate: catalysis by tertiary amines, *J. Am. Chem. Soc. 103*, 628−634.
23. Johnson, J. D., Creighton, D. J., and Lambert, M. R. (1986) Stereochemistry and function of oxaloacetate keto-enol tautomerase, *J. Biol. Chem. 261*, 4535−4541.

BI061688G